Observing Ocean Waves with Synthetic Aperture Radar

Luke Colosi

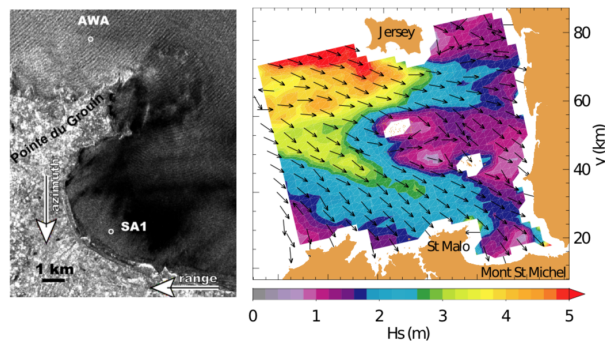SIOG 236: Satellite Remote Sensing Term Paper Part 3

June 23, 2020

Figure 1: Left: Sample of a SAR image, recorded by Envisat on March 9 2003, over French coast. Right: Full image processed into wave spectra, with significant wave height and peak direction (Ardhuin, 2020).

Contents

1 Introduction

Ocean surface gravity waves throughout the course of modern history have been vitally important for a broad range of human activities including commerce, fisheries, and human recreation. Furthermore, surface waves are fundamental to ocean–atmosphere interactions, and they mediate exchanges of momentum, heat, gasses, and energy (Cavaleri et al., 2012; Villas Bôas et al., 2019) which are key factors in Earth's climate system. Therefore, it is highly desirable to describe the wave field quantitatively and develop instruments to make these observations. To make these measurements, it important to understand complexities of the wave field and what is exactly generating these waves.

Surface waves with periods from 1 to 30 seconds are primarily generated by wind blowing over the surface of the ocean for a given distance and time period (Ardhuin, 2020). A single storm system over the ocean produce surface waves with a broad range of directions, wavelengths and amplitudes. At any given time in the ocean, there can be multiple storms or wind events generated the waves in a given region of the wave field. The waves produced from one of these wind events is call a wave system. Thus, the surface wave field consists of the superposition of a great number of plane waves each with their own particular direction, wavelength, and amplitude (Fig. 2) and each of these plane waves is associated with a particular wave system. Now we can ask what is the best way of describing this wave field?
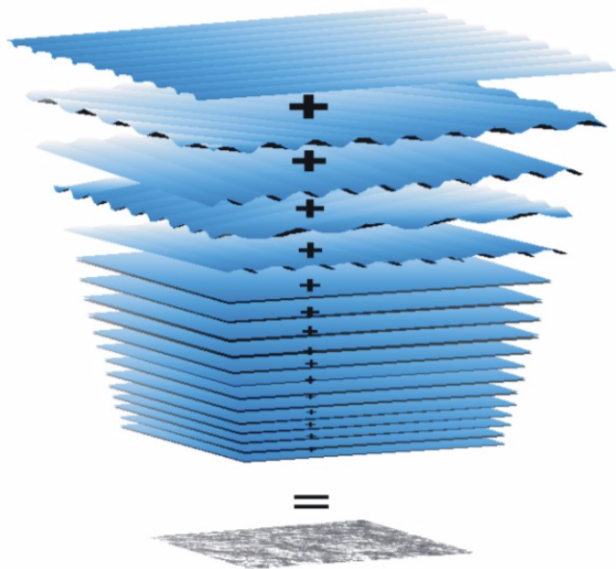

Figure 2: Superposition of a great number of plane waves giving us the sea state of the wave field (Ardhuin, 2020).

The wave field can be described using two metrics: Spectral and integral parameters. Spectral parameters include frequency, or direction frequency wave energy density spectrum, defined in its continuous form as:

$$E(f, \theta) = \lim_{\Delta f \to 0} \lim_{\Delta \theta \to 0} \frac{1}{\Delta f \Delta \theta} \left\langle \frac{1}{2} \rho_w g a_{ij}^2 \right\rangle \tag{1}$$

The direction frequency wave energy density spectrum tells us the energy observed in the wavefield of unit area for a wave of a given frequency coming from a particular direction. Fig. 3 illustrates a frequency spectrum (line plot) and a directional frequency spectrum (polar plot) obtained from a CDIP wave buoy off the coast of Hawaii. Alternatively, the wave field can be described using integral parameters which tell us the period, frequency, or direction of the highest energy waves in the wave field or for a particular wave system. In most cases, integral parameters are computed from the spectrum. Wave height can be also estimated through the convention of significant wave height.
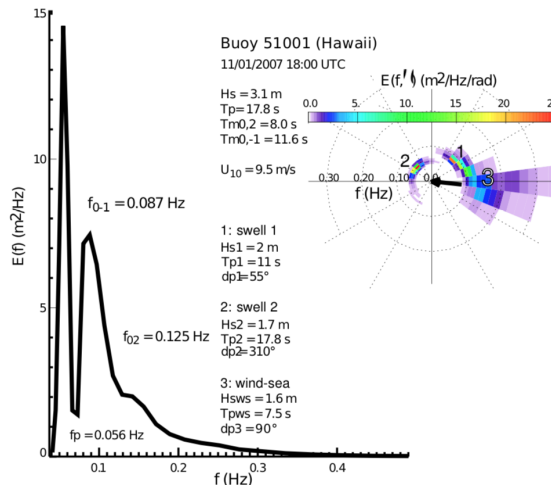

Figure 3: Frequency spectrum (line plot) and a directional frequency spectrum (polar plot) obtained by a CDIP wave buoy off the coast of Hawaii (Ardhuin, 2020).

Common instruments used to obtain these spectral and integral parameters include Wave buoys, bottom mounted sensors, and P–U–V Sensors. These sensors are obtain time records in–situ observations at a single point in space. To overcome this spatial limitation, radar remote sensing from space or aircraft can used. Some of these systems are limited to only obtaining integral parameters (i.e. radar altimetry), however some systems are able to observe wave energy density spectra. One of the suitable remote sensing systems is Synthetic Aperture Radar (SAR).

Here we undertake a detailed discussion on SAR remote sensing system and its application of observing ocean surface waves. We begin with SAR heritage and its developments over the decades. The general physical theory behind SAR measurements and the fundamental of observing ocean wave spectrum, practical operations specifics such as validation of observations, and data stream from the instrument are explored. An example is given for

the Sentinel-1A satellite to illustrate operations specifics of its SAR instrumentation. Lastly, an explanation for why SAR is best suited for measuring ocean wave spectra at global scales.

2   SAR Heritage and Improvements

SAR imaging was originally developed for application other than ocean science and branched out to many fields of Earth science including black and white aerial photography, cartography, vegetation mapping, generating digital elevation models (using SAR interferometry) and monitoring natural disasters such as floods and landslides (Rees, 2013).
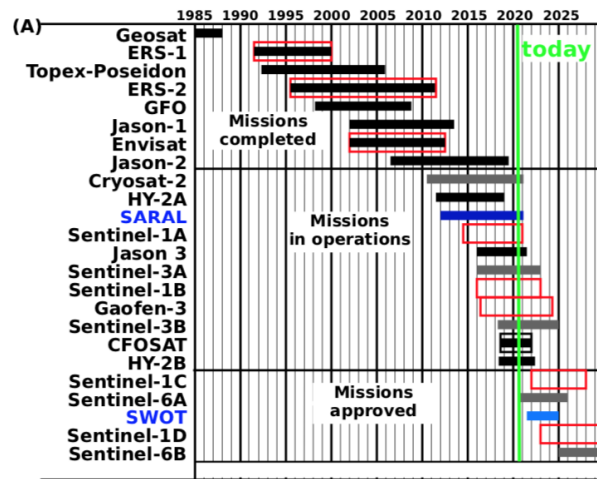

Figure 4: Satellite missions from 1985-2030 with altimeters: black solid bars, C-band SAR: red open boxes, Ku-band Real Aperture Radar: black open boxes, delay-Doppler Altimeters: grey solid bars (Ardhuin, 2020).

One of the first satellite missions with SAR sensors committed to imaging ocean surface waves was Seasat which was launched in 1978 (Lehner and Ocampo-Torres, 2003). Many scientists quested whether Seasat would be able to image ocean waves. However, images from Seasat L-band SAR data resolved distinct features of ocean waves including wave direction, and frequency spectra. This was a immense step forward from past optical radar techniques (Lehner and Ocampo-Torres, 2003). Seasat SAR images gave scientists the opportunity to develop imaging algorithms, and study ocean wave phenomena including refractions patterns and ray tracing from storm generation sites. Unfortunately, images each needed 8 hours processing time and Seasat had only a short campaign, failing after 100 days in operation due to a power short circuit (Hasselmann et al., 2012).

After the Seasat mission, there was a 13 year gap between the next satellite mission with SAR dedicated to observing surface waves. During this gap, several aircraft and shuttle missions including SIR B in 1984 and SIRC/X SAR in 1994 (Lehner and Ocampo-Torres, 2003) looked to further improve image processing algorithms for SAR and validation of SAR ocean wave measurements. The launch of the European Remote Sensing Satellite ERS-1 in 1991 marked the end of this 13 year gap. 5 by 10 km SAR images using C-band radiation from ERS-1 were able to image ocean waves with wavelengths larger than 100 m. However,

this lower bound restricted wave observations to only swell. Four years later, a near identical satellite ERS-2 was launched. Together, ERS-1 and -2 have large global coverage of the world oceans measuring waves in a wide variety of locations and conditions at a high resolution of up to 30 m in wave mode (Lehner and Ocampo-Torres, 2003). ERS SAR observations of ocean wave spectra has contributed significantly to spectral wave models such as the WAM model. However, onboard storage capabilities restricted the spatial coverage by limiting a single image to every 200 km along the satellite track (Lehner and Ocampo-Torres, 2003).

During the ERS satellite missions, Envisat was launched in 2002 (Lehner and Ocampo-Torres, 2003) which was equipped with the advance SAR (ASAR) sensor. In ENVISAT's wave mode, images of the ocean surface were obtained every 100 km in the along track direction. Envisat ensured the continuity of SAR data after ERS-2. Many other satellites including Sentinel-1A, Sentinel-1B, and Gaofen-3 have since been launched (Ardhuin, 2020) which have lead to further developments in our capabilities of observing the ocean surface waves from spaceborne satellite missions. Sentinel-1 series improved revisit time, geographic coverage and rapid data distribution from its predecessor. Future satellites that will be equipped with SAR instrumentation are Sentinel-1C and -1D with launch dates planned for 2022 and 2023 respectively. The SAR satellite legacy beginning with ERS-1 is shown in Fig. 4.

3   Theoretical Principles of SAR

3.1   SAR Fundamentals

SAR is a type of active microwave instrumentation that uses backscattered power and phase to produce high resolution images of earth's surface (Rees, 2013). Microwave electromagnetic radiation is used because of its ability to penetrate through clouds and operate without sunlight allowing SAR to capture images in a wide variety of conditions (Hasselmann et al., 2012). Fig. 5 illustrates the side-looking geometry of the SAR sensor in orbit. By convention, the along track direction of the satellite is known as the azimuth direction while the across track directions is know as the range direction. The distance from the antenna to the center of the footprint is know as the slant-range distance. We will begin with a brief synopsis of SAR imaging process over an arbitrary surface with a discuss the azimuth and range resolution and pulse repetition frequency. Lastly, the distortions and modulations caused by a complex surface will be discussed along with corrections and interpretations of SAR image.

Initially, the SAR antenna emits short pulses of microwave radiation towards the earth surface from an oblique looking angle (Fig 5). The radiation interacts with the surface depending on the surface roughness, dielectric constant, and topographic orientation causing the radiation to either specular, quasi-specular, diffuse or bragg scatter off the surface. A fraction of the radar pulse is backscattered (or echoed) off the surface towards the satellite. At the satellite, coherent backscattered radiation's amplitude (intensity) and phase (range) are recorded (Sandwell et al., 2011) from the illuminated area within the satellite's swath called the satellite's footprint. The size of the foot print in the azimuth and range directions are limited by the beamwidth of the antenna as seen in Fig. 6. Consider the SAR antenna in
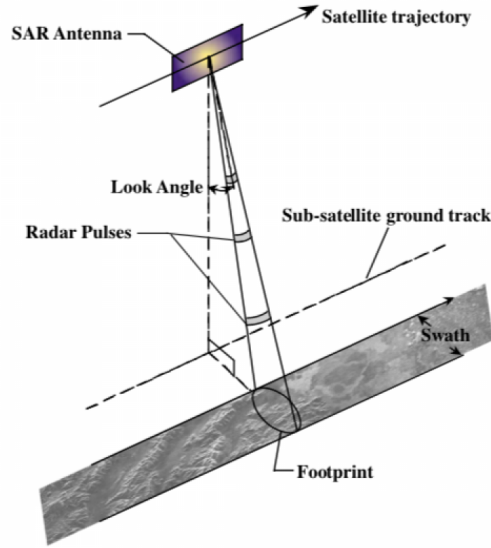
Figure 5: Satellite geometry between the antenna and earth's surface (Sandwell et al., 2011)

Fig. 6 with length L in the azimuth direction and w in the range direction. By the diffraction limit on the spatial resolution, we can state:

$$\beta \approx \frac{\lambda}{L} \tag{2}$$

$$\psi \approx \frac{\lambda}{w} \tag{3}$$

where λ is the wavelength of the incident radiation. High spatial resolution in the range direction is attained by transmitting very short pulses towards the surface. If the duration of the radar pulse is t_p, two scatterers on earth's surface can be resolved given that their distances from the radar differs by at least $\frac{ct_p}{2}$ where c is the speed of light in free space. This is known as the slant range resolution Δs. The range resolution as seen in Fig. 6 is given by:

$$R_r = \frac{ct_p}{2\sin\theta} \tag{4}$$

where θ is the looking angle. From equation (4), we can see that shortening the duration of the radar pulse t_p increases the resolution in the range direction. If $\theta = 0$ such that the SAR antenna was looking nadir, the R_r would approach infinity. This means that nothing can be resolved in the range direction. This is why the SAR antenna must oriented at a side-looking prospective of earth's surface. Notice that the range resolution is independent of the satellite's height and the wavelength of the radiation. The azimuthal resolution is limited by the beamwidth β of the antenna as defined in equation (2). We can approximate the azimuth resolution by the arc length relation to the distance from the center of the radar pulse to the satellite s and the subtending angle β:

6

$$R_a \approx s\beta \approx \frac{H}{\cos\theta} \times \frac{\lambda}{L} = \frac{H\lambda}{L\cos\theta} \tag{5}$$

Therefore, for side-looking radar systems, the azimuthal resolution is dependent on the altitude of the satellite H and the length of the antenna. For SAR mounted on spacecraft, H is very large. In order for the satellite to be able to resolve surfaces in the azimuth direction, the antenna's length L must be unrealistically long. However, SAR solves this problem by utilizing the motion of the satellite. Given that the satellite is travelling at a velocity v over the time interval T, by recording signals collected over the distance $L = vT$, a larger aperture can be synthesized reconstruct the signal over the distance L. This is done by coherently summing images in the azimuth direction. This is why SAR is names synthetic aperture radar. Because the satellite is orbiting at $\sim O(700km)$, this time interval T is on the order of seconds. the length of the synthetic aperture becomes $L' = 2R_a$ which gives us a azimuthal resolution of:

$$R_a = \frac{H\lambda}{(2R_a)\cos\theta} = \frac{H\lambda}{2\frac{H\lambda}{L\cos\theta}\cos\theta} = \frac{L}{2} \tag{6}$$

This tells us that as we decrease the antenna length in the azimuth direction, the azimuth resolution improves. However, the resolution of SAR images is constrained by the pulse repetition frequency (PRF). PRF has the following lower and upper bounds:

1. **Minimum PRF**: A new pulse can only be sent out every $\frac{L}{2}$ to avoid aliasing the image (i.e. not forming a complete image of earth's surface). Mathematically speaking: PRF$> \frac{2V}{L}$.

2. **Maximum PRF**: When we send out a pulse, it sweeps its way across the swath from near to far range. We cannot send out another signal until the first pulse has reached the far range to avoid ambiguity (i.e. scrabbling the near range single of the new pulse with the far range signal of the old pulse). Mathematically speaking: PRF$< \frac{c}{2H}\sec\theta_2\sec\theta_1$.

The PRF introduces a swath width and azimuthal resolution dependence such that decreasing L leads to an increase in PRF to satisfy the lower bound condition. However, the swath narrows in the azimuth direction to satisfy the upper bound condition.

When the backscattered radiation reaches the satellite, the raw signal data is stored in a file. SAR image formation requires two processing steps. First, onboard satellite processing which demodulating and digitizing return signal for transmission. Second, once the signal is transmitted, a computer program called the digital SAR processor converts the raw signal data into a focused single-look complex (SLC) image in physical space. Each pixel in SLC image is complex number that represents an echo from a fixed scatterer on the surface. The origin of the echo is determined in the range direction by range gating of return signal and in the azimuth direction by the Doppler shift of the scattered signal. This single–look complex image is then used to obtain backscatter intensity σ_0 or phase images.

SAR images subject to multiple distortion due to the non-trivial features on Earth's surface. These distortions come in three main forms: Geometric, radiometric, and target–motion. Geometric are caused by topographic features and include slant–range, layover, and
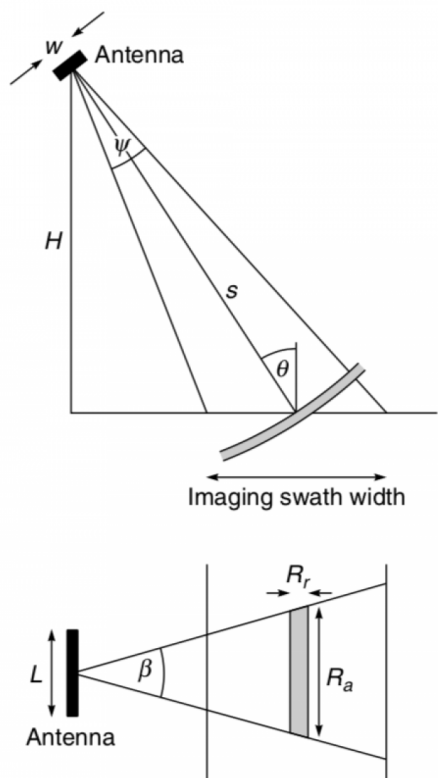
7

Figure 6: Geometry of a side-looking radar system viewed from behind the platform flying into the page (top figure) and above with the platform flying up the page (bottom figure) (Rees, 2013)

foreshortening distortions. Radiometric are caused by the antenna pattern bias (higher focus in the center of the image from illumination pattern from Fraunhofer diffraction pattern). Target–motion leads to azimuthal shift from a secondary Doppler effect from relative velocity of target in the direction of the satellite.

3.2   Principles of Observing Ocean surface waves with SAR

For the ocean surface, the fraction of the radar pulse is backscattered via Bragg scattering off the ocean surface by ocean waves with wavelengths on the same order of magnitude as the incident radiation back toward the satellite. Because the radar's wavelength for ocean wave SAR satellites are usually in C-band, $7.5 < \lambda_r < 3.5$ cm which means surface capillary waves are the primary scatterers of microwave radiation from the satellite. Unlike land terrain SAR imaging, the entire complex surface topography of the ocean sea surface is moving. This causes the SAR image over the ocean to experience significant distortions from geometric and target-motion induced distortions. Therefore, SAR images of the ocean suffer three types of distortions:

1. **Hydrodynamic modulation** : Waves modulate the amplitude and thus the backscatter intensity

2. **Tilt modulation** : Waves modulate the local geometry and slopes of the sea surface

3. **Velocity bunching** : Wave orbital velocities in the direction of the satellite (vertical and horizontal) causing a azimuthal shift in an echo's position and leading to bright areas where displaced targets are bunched together.

Velocity bunching is the main cause of wave induced modulation of and causes the image to be in range-Doppler space rather than physical space. The location of the target is just shifted in the azimuthal direction, because the location of the echo is determined by the Doppler shift. There is a second Doppler shift in the case where both the platform and the target are moving causing a miscalculation in the echo's location. For example, suppose we have a monochromatic wave train with wavenumber k_y propagating in the azimuthal (y) direction at a incidence angle θ from the SAR antenna (Ardhuin, 2020). The displacement in the azimuth direction due to velocity bunching would be:

$$\delta = (W \cos(k_y y - \sigma t) \cos(\theta) + U \sin(k_y y - \sigma t) \sin(\theta)) \times \frac{H_r}{V \cos(\theta)} \tag{7}$$

where $\vec{u} = (U, W)$ is the orbital velocity of the wave in the horizontal and vertical directions respectively, σ is the wave frequency, H_r is the altitude of the satellite, and V is the ground velocity of the satellite. The first term in equation (7) accounts for the azimuthal shift due to the vertical motion towards the satellite and the second term accounts for the azimuthal shift due to the horizontal motion towards the satellite. Fig. 7 shows velocity bunching effects on the location of the wave for a range of wave heights. Fig. 7 illustrates well the fact that as wave steepness increases or wave height increases, velocity bunching intensifies.
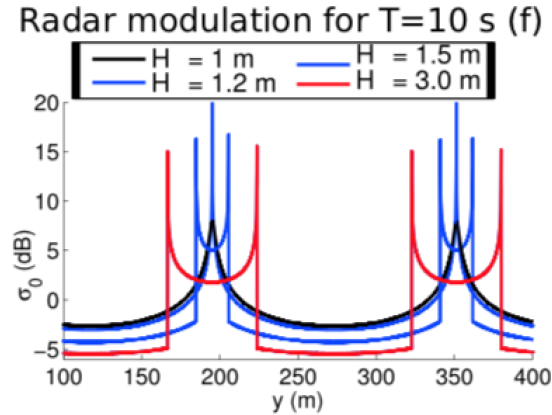

Figure 7: Velocity bunching azimuthal shift example for a sinusoidal monochromatic wave of wavelength 156 meters with varied wave height H (Ardhuin, 2020).

In order to extract the ocean wave 2D-directional spectrum from the SAR image, we need to correct the image from these three types of distortions. One way of doing this is using a "first guess" algorithm introduced by Hasselmann and Hasselmann (1991). This method take advantage of the fact that the hydrodynamic, tilt and velocity bunching modulation of the SAR Images can be represented by linear transfer functions. The hydrodynamic and tilt

9

transformations are reasonably well understood understood, however, the velocity bunching transform becomes quickly nonlinear when wave steepness increases and the direction of propagation of the satellite becomes parallel with the direction of wave propagation. With the combined effects of these two limiting cases, the SAR image of the sea surface becomes smear out. This means the "first guess" algorithm is more challenging to perform when the wave field is dominated by wind seas (steep locally forced waves) or high wave height. The general logic of the algorithm is captured in the following steps (Fig 8):

1. **Step 1**: Obtain a first guess wave spectrum from a wave model in the region where the SAR image is taken. Compute two–dimensional wavenumber SAR image spectrum from the SAR image.

2. **Step 2**:Nonlinearly transformed first guess spectrum (via the linear combination of modulation transfer functions) to an associated SAR image spectrum.

3. **Step 3**: Apply a maximum-likelihood matching between the observed and associated SAR image spectra.

4. **Step 4**: Remove regions of the SAR image spectrum which are strongly distorted from three types of image distortions.

These steps are graphically shown in Fig. 8. The downfall of this method is its dependence on needing a first guess spectrum of the wave field to correct the SAR image spectrum. Others (Mastenbroek and De Valk, 2000) have developed spectral inversion algorithm that utilizes wind vector measurements from scatterometers onboard spacecraft to fill in missing spectral information. The theory of the SAR imaging of ocean waves is comprehensively outlined in the results from the Marine Remote Sensing Experiment (MARSEN) (Hasselmann and Hasselmann, 1991). The theory is presented here as an simplified overview.
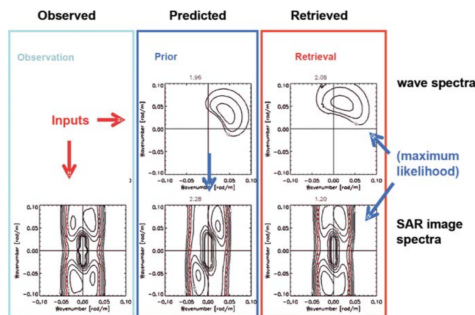

Figure 8: Graphical depiction of the "first guess" algorithm from Hasselmann et al. (2012).

An additional limitation of SAR images of the ocean are high frequency surface waves. These short wave length waves for SAR processing are equivalent to Gaussian random vertical oscillations of $\langle v^2 \rangle$ which manifest as random displacements in the SAR image. Therefore, short waves do not produce any pattern in the SAR image. The wavelength that marks the boundary between resolved and non-resolved surface waves is known as the azimuthal cut–off wavelength which is defined as:

$$\lambda_c = \frac{2\pi\sqrt{\langle v^2 \rangle}H_r}{V} \tag{8}$$

where $\langle v^2 \rangle$ is the orbital velocity variance, V is the velocity of the satellite, and H_r is the altitude of the satellite. These short waves cause a reduction in the contrasts between longer wavelength waves by an exponential factor $E_s(\mathbf{k}) = e^{(-k_y^2\langle v^2 \rangle\frac{H_r}{V})}E_l(\mathbf{k})$ where $E_s(\mathbf{k})$ is the two dimensional wavenumber SAR image spectrum and $E_l(\mathbf{k})$ is the associated two dimensional wavenumber SAR image spectrum from the "first guess" wave model Ardhuin (2020). The short wavelength waves lead to an overall blurring to the SAR image.

In order to obtain the directional spectrum from SAR imagery, multiple images of the sea surface from successive looks must be taken to resolve the directional ambiguity in the measurements (Hasselmann et al., 2012). This is done using multi-look SAR data. Given several successive images of the wave field, the differences between the images due to the propagation of the wave can be quantified by computing the cross spectrum between each image. The real part of the cross-spectrum gives an idea about the amplitude while the imaginary part give use intuition about the phase difference between the two images. By extracting the information from the cross-spectrum between successive looks, the full directional spectrum can be obtained. Further theory discussing how to compute the directional wave spectrum can be found in Jackson et al. (1985).

4   Specifics on Operations in Orbit

4.1   Validating Observations

Validation of SAR spectra obtained from various algorithms including the inverse algorithm presented here could be done by possible comparing in-situ wave spectra observations with SAR derived wave spectra during the Calibration and Validation phase of the satellite's mission. After calibration and validation, the measurements are considered robust and accurate. However, sensor drift and other uncertainties must be addressed during image processing. I will need to do more research on this ground truth validation.

4.2   Data onboard storage and transmission from the Instrument

As mentioned above, onboard storage of high resolution SAR imagery presents a challenge for continuous coverage of the ocean surface. The generation data from continuous operation at high spatial resolution is at too fast a rate such that the data quantity is too large to be stored onboard the spacecraft. Moreover, the transmission to sparsely located ground station also places a limit on the amount of data that can be collected. To solve these problem, satellites such as ERS and ENVISAT alternating the SAR sensor between two modes: a standard broad-swath mode and a global SAR wave mode. The standard broad-swath mode would be turned on when the sub-satellite point enters the station mask of the satellite's receiving station. With direct connection to the ground station, the satellite is able to collected large high resolution images spanning the entire swath and transmit them directly to the ground station. When the satellite is not in direct line of sight with the

ground station, the SAR is placed in wave mode which periodically activated the sensor for short periods every 200 km to 100 km along the orbit. During these periods, 5×10 km rectangular 'imagettes' are produced which capture a small fraction of the swath as seen in Fig. 9. Using wave mode allowed the satellite to store data onboard the satellite and transmit it once in sight of a ground station. These 'imagettes' cover large regions of the earth's on a order much greater than the wavelengths of ocean waves which ensures meaningful statistical ocean wave spectrum.
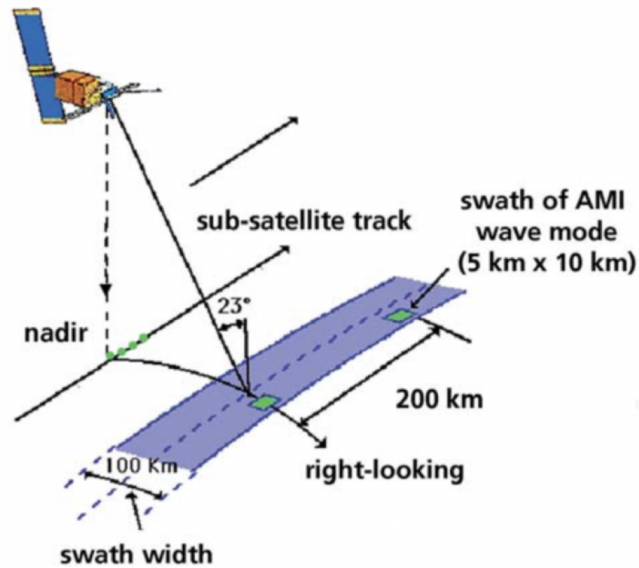

Figure 9: The SAR active microwave instrument (AMI) in wave mode for ERS-1 and -2.

5   Case Study: Sentinel-1A

In order to provide a more practical approach for working with SAR imagery and putting the theory into action, a case study of Sentinel-1A SAR instrumentation is provided. Information and user guide comes from the European space agency website. For a quick overview, Sentinel-1A's SAR operating in single or dual polarization uses C-band microwave radiation ($\lambda = 5.5cm$) for imaging the ocean surface to obtain SAR SLC images. 2D-wave spectrum and the wave field's integral parameters such as peak period and significant wave height are obtained after further processing SAR SLC images. When not over the open ocean, many land measurements are made. Sentinel-1A has four modes which includes stripmap, Interferometric Wide swath, Extra-Wide swath (3 land modes), and wave mode (Fig. 10). Wave mode acquired 20 by 20 kilometer imagettes every 100 km at two different incident angles. Data processing levels range from 0 to 2 where:

1. **Level 0**: Raw unprocessed data of SAR images

2. **Level 1**: Includes processed single-look complex (SLC) data of imagery and ground range detected (GRD) with multi-looked intensity images

3. **Level 2**: Ocean data of retrieved geophysical parameters after full processing SAR image. Includes ocean swell spectra (OSW), Ocean Wind Fields (OWI) and Surface Radial Velocities (RVL)

The on broad storage capacity is 1410 Gigabytes with download link capacity of $520 \frac{Mbits}{s}$. For more information, the full user guide with explanations for algorithms for processing SAR imagery is give on their website.
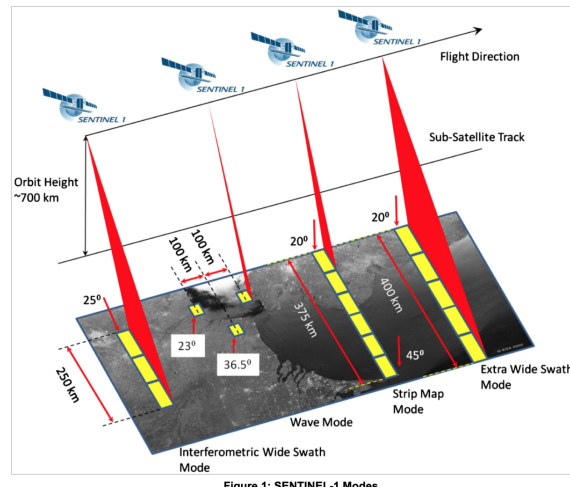

Figure 10: Sentinel-1 Acquisition modes and Orbital parameters.

5.1 Data Analysis of Level 1 and 2 Products

In order to understand how these sentinel-1 products are structured and the initial steps in order to preform data analysis on SAR images, I downloaded level 1 SLC wave mode and level 2 ocean wave spectrum SAR data from Copernicus Open Access Hub. This site provides level 1 (SLC) and 2 (OCN) data in a graphical user interface or an API. Data can be selected in large swaths containing multiple SAR images on a global map in the GUI. Going into the directory measurements allows you to select individual SAR images. For SLC, the SAR image is in a geotiff file. After downloading the image onto your computer, the file can be uploaded onto a computer program (i.e. python) and convert the geotiff file to a workable data format. For Sentinel-1 data, IFREMER outlines well the libraries to preform this conversion along with sample code. For an example, Fig. 11 illustrates an amplitude SAR image with two two steps of smoothing to reduce speckle noise.

Observe, that I need to use low pass filtering to remove speckle noise. However, I was not able to really resolve any wave modulation features in any of the SAR images in Fig. 11. This is possible due to the wave field having more high frequency waves (i.e. wind seas) which are not resolved well. Additionally, the low amount of image processing preformed limited the amount I can see. Figs. 12, 13, 14 display the level-2 OCN data's ocean wave energy directional frequency and cross spectrum.
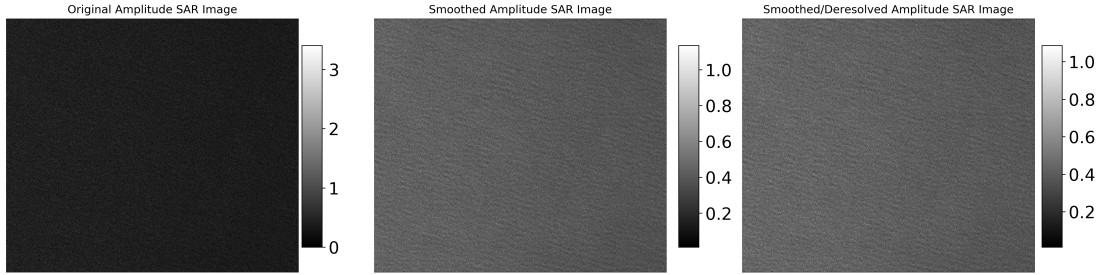
13

Figure 11: Amplitude of SLC image with increasing amounts of low pass filtering from the North Pacific Ocean June 6th, 2020 (left to right: no filter, 5 by 5 pixal running mean, 5 by 5 pixal running mean and 5 by 5 zoom).
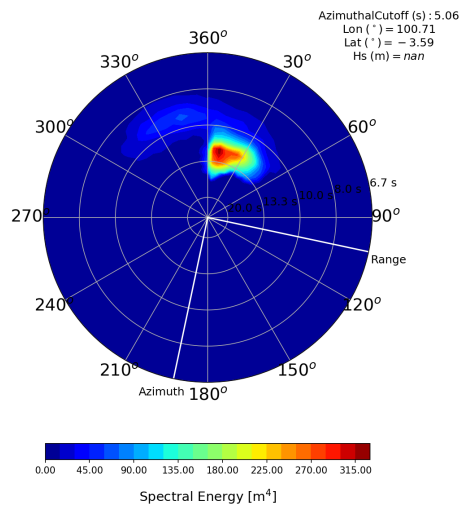

Figure 12: Directional–frequency wave energy density spectrum from Sentinel 1A over the North Pacific Ocean on June 6th, 2020.

6 Why is SAR well suited to this application?

SAR is a well suited instrument for obtaining 2D ocean wave spectra because it obtains large global coverage of high resolution SAR images which can be converted into wave spectra using the techniques outlined here. In addition, due to the high transmissivity of microwave radiation through the atmosphere and independence from light, the SAR active microwave system is robust and versatile for many weather conditions. However, there are many limitations that which make SAR not as ideal for observing ocean spectra. These include the lack of continuous operation, computationally taxing image processing, the inability to observe shorter period waves due to velocity bunching, and azimuthal cutoff angle. However, SAR have made an invaluable contribution to the field of physical oceanography such as helping to improving wave models despite its limitations. A few applications of SAR data include surface Wave refraction in coastal waters (Collard et al., 2005), computation of Bulk wave parameters in coastal and open-ocean regions (Collard et al., 2005), and observation of ocean
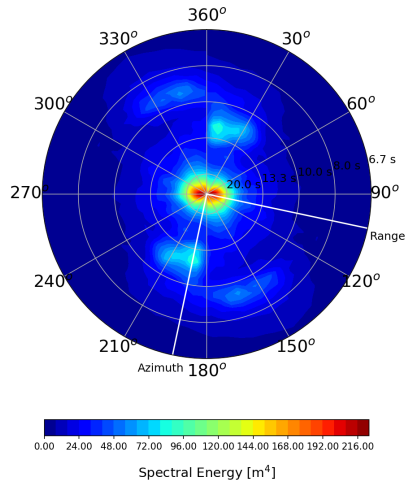
Figure 13: Real part of Cross-spectrum from Sentinel 1A over the North Pacific Ocean on June 6th, 2020.

waves in sea-ice (Ardhuin et al., 2015).

7 Conclusion

To conclude, we have discussed in detail observing ocean waves using synthetic aperture radar. Even though limitations of directional frequency wave energy density spectrum derived from SAR seem extensive, there has been great progress in understanding SAR images over the ocean in a wide variety of conditions and many great studies preformed utilizing SAR data. SAR image interpretation is still an active field of research and algorithms for SAR image processing are still being explored.

To explore SAR images from the Sentinel-1 campaign, the French Research Institute for Exploitation of the Sea (IFREMER) provides an easy-to-use and comprehensive interface found here on their website.

References

Ardhuin, F., Collard, F., Chapron, B., Girard-Ardhuin, F., Guitton, G., Mouche, A., and Stopa, J. E. (2015). Estimates of ocean wave heights and attenuation in sea ice using the sar wave mode on sentinel-1a. *Geophysical Research Letters*, 42(7):2317–2325

Ardhuin, F. (2020). *Ocean waves in geosciences*

Cavaleri, L., Fox-Kemper, B., and Hemer, M. (2012). Wind waves in the coupled climate system. *Bulletin of the American Meteorological Society*, 93(11):1651–1661
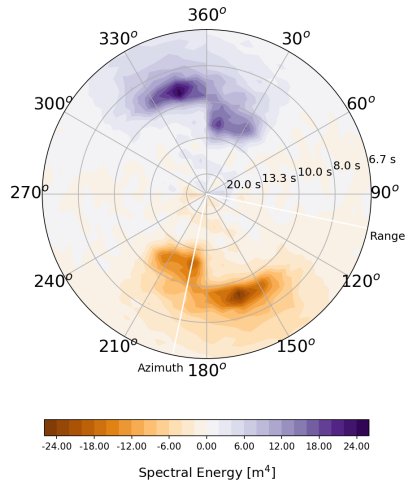
Figure 14: Imaginary part of Cross spectrum from Sentinel 1A over the North Pacific Ocean on June 6th, 2020.

Collard, F., Ardhuin, F., and Chapron, B. (2005). Extraction of coastal ocean wave fields from sar images. *IEEE Journal of Oceanic Engineering*, 30(3):526–533

Hasselmann, K., Chapron, B., Aouf, L., Ardhuin, F., Collard, F., Engen, G., Hasselmann, S., Heimbach, P., Janssen, P., Johnsen, H., et al. (2012). The ers sar wave mode–a breakthrough in global ocean wave observations

Hasselmann, K. and Hasselmann, S. (1991). On the nonlinear mapping of an ocean wave spectrum into a synthetic aperture radar image spectrum and its inversion. *Journal of Geophysical Research: Oceans*, 96(C6):10713–10729

Hasselmann, K., Chapron, B., Aouf, L., Ardhuin, F., Collard, F., Engen, G., Hasselmann, S., Heimbach, P., Janssen, P., Johnsen, H., et al. (2012). The ers sar wave mode–a breakthrough in global ocean wave observations

Jackson, F. C., Walton, W. T., and Baker, P. L. (1985). Aircraft and satellite measurement of ocean wave directional spectra using scanning-beam microwave radars. *Journal of Geophysical Research: Oceans*, 90(C1):987–1004

Lehner, S. and Ocampo-Torres, F. (2003). The sar measurement of ocean waves: wave session whitepaper. *ESA-SP Series, this issue*

Mastenbroek, C. d. and De Valk, C. (2000). A semiparametric algorithm to retrieve ocean wave spectra from synthetic aperture radar. *Journal of Geophysical Research: Oceans*, 105(C2):3497–3516

Rees, W. G. (2013). *Physical principles of remote sensing.* Cambridge university press

Sandwell, D., Mellors, R., Tong, X., Wei, M., and Wessel, P. (2011). Gmtsar: An insar processing system based on generic mapping tools

Villas Bôas, A. B., Ardhuin, F., Ayet, A., Bourassa, M. A., Brandt, P., Chapron, B., Cornuelle, B. D., Farrar, J., Fewings, M. R., Fox-Kemper, B., et al. (2019). Integrated observations of global surface winds, currents, and waves: Requirements and challenges for the next decade. *Frontiers in Marine Science*, 6